Sonochemical Preparation of Nanosized Amorphous $NiFe_2O_4$ Particles

Kurikka V. P. M. Shafi, Yuri Koltypin, and Aharon Gedanken*

Department of Chemistry, Bar-Ilan University, Ramat-Gan 52900, Israel

Ruslan Prozorov

Department of Physics, Bar-Ilan University, Ramat-Gan 52900, Israel

Judit Balogh

Research Institute for Solid State Pysics, P.O. Box 49, H-1525, Budapest, Hungary

Janos Lendvai

Department of General Physics, Lorand Eotvos University, Budapest, Hungary

Israel Felner

Racah Institute of Physics, Hebrew University, Jerusalem 91904, Israel

Received: March 11, 1997; In Final Form: June 4, 1997[⊗]

Nanosized amorphous $NiFe_2O_4$ powder was prepared by sonochemical decomposition of solutions of volatile organic precursors, $Fe(CO)_5$ and $Ni(CO)_4$, in decalin at 273 K, under an oxygen pressure of 100−150 kPa. The amorphous nature of these particles was confirmed by various techniques, such as SEM, TEM, electron microdiffraction, and X-ray diffractograms. Magnetic measurements, Mössbauer, and EPR spectral studies indicated that the as-prepared $NiFe_2O_4$ ferrite particles were superparamagnetic. The Mössbauer spectrum of the crystallized sample showed a clear sextet pattern, with hyperfine field values of 500 and 508 kOe for A (tetrahedral) and B (octahedral) sublattices, respectively, of the inverse spinel $NiFe_2O_4$. Saturation magnetization of the annealed sample (25 emu/g) was significantly lower than that for the reported multidomain bulk prticles (55 emu/g), reflecting the ultrafine nature of the sample. Thermogravimetric measurements with a permanent magnet gave Curie temperatures of 440 °C for amorphous and 560 °C for the crystallized forms.

Introduction

Ferrites are a group of technologically important magnetic materials of current interest. Their applications include fabrication of magnetic cores of read/write heads for high-speed digital tape or disk recording.[1,2] Nanostructured materials are now being studied intensively, as their physical properties are quiet different from those of the bulk.[3,4] A variety of methods have been used to prepare nanosized ferrite particles. The conventional high-temperature ceramic method for the preparation of ferrites can result in the loss of their fine particle nature. The wet chemical methods include coprecipitation,[5−7] spray drying,[8] and hydrothermal processes.[9] The fine ferrite particles are also produced by grinding coarse powders of high-purity bulk material in the presence of kerosene and oleic acid (organic surfactant).[10] However, in this method, the oleic acid is strongly bonded to the surface, making it difficult to remove by chemical means. Surfactant microstructures (reverse micelles) have also been used to synthesize nanosized ferrite particles.[11,12]

Amorphous materials, obtained by rapid quenching of the melt, have many important applications. Iron-based amorphous oxides exhibiting ferromagnetic character, with a Curie point higher than room temperature and relatively high saturation magnetization, are of great importance because of their unique electronic and magnetic properties. They can be used in magnetooptical devices such as optical isolators, optical switches, etc.[13] Amorphous ferrites, in flake form, had been prepared by rapidly quenching the molten mixtures of bulk mother ferrite with one or two kinds of glass formers, such as P_2O_5, V_2O_5, MoO_3, SiO_2, Bi_2O_3, etc., as an additive to prevent crystallization.[14,15] Bulk $NiFe_2O_4$ is a soft ferrimagnetic material with completely inverse spinel structure. In this paper, we discuss the sonochemical synthesis and characterization of nanosized amorphous $NiFe_2O_4$ powder which does not require any glass former.

Acoustic cavitation, i.e., the formation, growth, and implosive collapse of a bubble in an ultrasonically irradiated liquid, generates a transient localized hot spot, with an effective temperature of 5000 K and a nanosecond lifetime.[16−18] The rapid cavitational cooling rate ($>10^9$ K s^{-1}) is much greater than that obtained by the conventional melt-spinning technique[19] for the preparation of metallic glasses ($10^5−10^6$ K s^{-1}). Since the thermal conductivities of metal oxides are usually much lower than those of the metals, faster cooling rates are needed to prepare amorphous metal oxides, and this is the reason that glass formers, which can prevent crystallization, are employed during the quenching process.

The foremost criterion for achieving a good sonochemical yield is that the precursor be volatile, because the primary sonochemical reaction site is the vapor inside the cavitation bubbles.[20] Secondly, the solvent vapor pressure should be lower at the sonochemical temperature, since the solvent vapor inside the bubble reduces the collapse efficiency. Suslick et al. employed this new sonochemical method for the preparation of nanosized amorphous powders of Fe, Co, and their alloys[21−23]

* Corresponding author. Fax: +972-3-5351250. E-mail: gedanken@ashur.cc.biu.ac.il.

[⊗] Abstract published in *Advance ACS Abstracts,* July 15, 1997.

S1089-5647(97)00893-6 CCC: $14.00

and metal carbide, Mo_2C.[24] Using polymeric ligands like poly(vinylpyrrolidone) (PVP) or oxide supports (alumina or silica), these nanosized clusters can be trapped as colloids or supported catalysts, respectively.[25] We have reported the preparation of amorphous Ni powder by sonochemical decomposition of nickel tetracarbonyl $Ni(CO)_4$, as neat liquid or solution in decalin.[26] By varying the precursor $Fe(CO)_5$, we were able to control the particle size of amorphous Fe.[27] Nanosized amorphous powders of γ-Fe_2O_3 and Fe−Ni alloy were also prepared by the sonochemical method.[28,29]

Experimental Section

Iron pentacarbonyl (Aldrich) was used without further purification. Nickel tetracarbonyl (Pfaltz and Bauer, Inc.) was distilled prior to use. *Nickel tetracarbonyl is a highly poisonous liquid with high vapor pressure. It is very sensitive to air and moisture, so care should be taken in handling it.* Pentane (Fluka) and decalin (Sigma) were dried with sodium metal or a 4 Å molecular sieve and stored inside a glovebox. The precursor solution was degassed by purging with high-purity argon (<10 ppm O_2) prior to sonication.

The $NiFe_2O_4$ was prepared by ultrasonic irradiation of the solution of $Fe(CO)_5$ and $Ni(CO)_4$ in decalin at 273 K, under 100−150 kPa (1−1.5 atm) of oxygen, with a high-intensity ultrasonic probe (Sonics & Materials, Model VC-600, 1.25 cm Ti horn, 20 kHz, 100 W/cm^2). After 3 h of irradiation, a black powder was obtained, which was then centrifuged and washed with dry pentane inside the glovebox. Centrifuging and washing were repeated at least five times, and finally the product was dried under vacuum.

Powder X-ray diffractograms were recorded on Rigaku X-ray diffractometer (Cu Kα radiation, $\lambda = 0.154\ 18$ nm). Scanning electron micrographs and energy dispersive X-ray analysis (EDX) were carried out on JEOL-JSM-840 electron microscope. Transmission electron micrographs were obtained with a JEOL-JEM100SX electron microscope. Magnetization loops were measured at room temperature using an Oxford Instrument vibrating sample magnetometer. The surface area (BET method) was measured on a Micromeritics-Gemini surface area analyzer. Mössbauer spectroscopic studies were carried out using a conventional constant acceleration spectrometer with a 50 mCi ^{57}Co:Rh source. Variable temperature ESR spectra were recorded on a Bruker ER 041 spectrometer operating at X-band frequency ($\nu = 9.7$ GHz) with 100 kHz magnetic field modulation. Magnetic force measurements were carried out on Mettler TGA4000 with a small permanent magnet. Differential scanning calorimetry (DSC) thermograms were obtained on a Mettler-Toledo calorimeter at a heating rate of 10 °C/min under flowing, pure nitrogen (50 mL/min). All sample preparation and transfer for these measurements were done inside the glovebox.

Results and Discussion

We have noticed that the sonochemical efficiency for the decomposition is less for $Fe(CO)_5$ than for $Ni(CO)_4$,[29] so it is necessary to use an initial excess of $Fe(CO)_5$ to get $NiFe_2O_4$. The poor reactivity of $Fe(CO)_5$ compared to $Ni(CO)_4$ can be traced to its lower vapor pressure when compared to $Ni(CO)_4$. For example, at 293 K, the vapor pressure of $Ni(CO)_4$ is 44.3 kPa (332 Torr), whereas it is only 2.8 kPa (21 Torr) for $Fe(CO)_5$ at the same temperature. There are two regions of sonochemical reactivity in ultrasonically irradiated liquids, one corresponding to the gas phase within the collapsing cavity and the second to a thin liquid layer immediately surrounding the collapsing cavity.

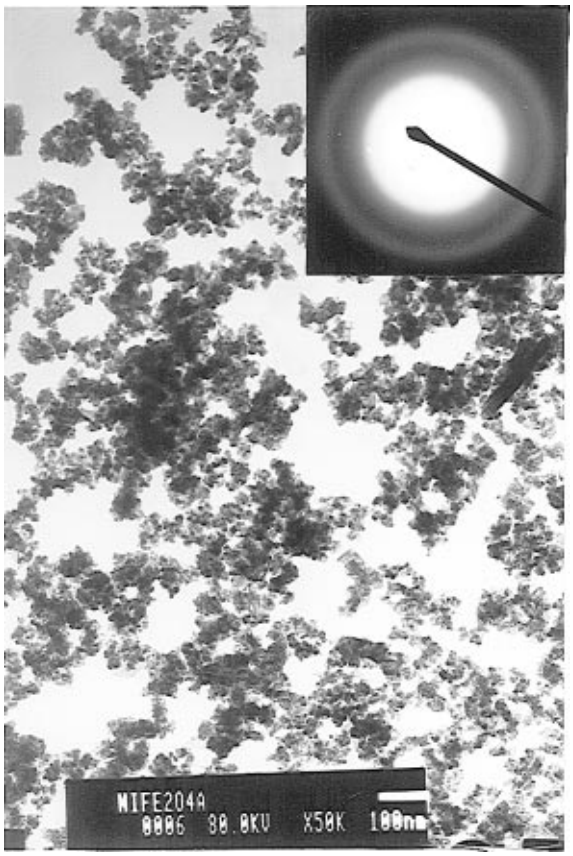

Figure 1. TEM image with microdiffraction (inset) for amorphous $NiFe_2O_4$.

The observed sonochemical reactivity on metal carbonyl vapor pressure is expected for reactions occurring in the gas phase. As the precursor's vapor pressure increases, its concentration within the gas-phase cavity increases linearly, thus increasing the observed sonochemical reaction rate.

Ferrite composition was determined by elemental and EDX analyses. Since the atomic numbers of Ni and Fe are similar, the ratio of the X-ray intensities from these elements approximates their composition. The intensity ratio of Fe:Ni as detected by the EDX is 2:1. Since these particles are much smaller than the free path for X-ray transmission through solids, i.e., 100 nm, the X-ray intensities need not be corrected for absorption and fluorescence effects.

The elemental analysis shows that the amorphous $NiFe_2O_4$ powder has trace amounts of carbon (<6%) impurities. The presence of carbon is presumably a result of the decomposition of alkane solvents or adsorbed CO during ultrasonication, and this probably plays an important role in stabilizing the amorphous structure.[29]

The amorphous nature of the particle was confirmed by various techniques, such as SEM, TEM, electron microdiffraction, and X-ray diffractograms. A scanning electron micrograph of $NiFe_2O_4$ powder shows coral-like features typical for noncrystalline materials.[21] The TEM images of the as-prepared and heat-treated samples of $NiFe_2O_4$ are shown in Figures 1 and 2. Figure 1 gives no evidence of crystallite formation and shows that the as-prepared material is an agglomerate of nanoparticles with diameters <10 nm. Most of the particles are aggregated in a spongelike form, so is difficult to determine the particle size exactly. The TEM microdiffraction pattern (inset) shows only diffuse rings characteristic of amorphous materials. However, Figure 2 clearly shows nearly uniform spherical ferrite particles with sizes less than 25 nm. The ED pattern (inset) reflects that these nanoparticles are well crystal-

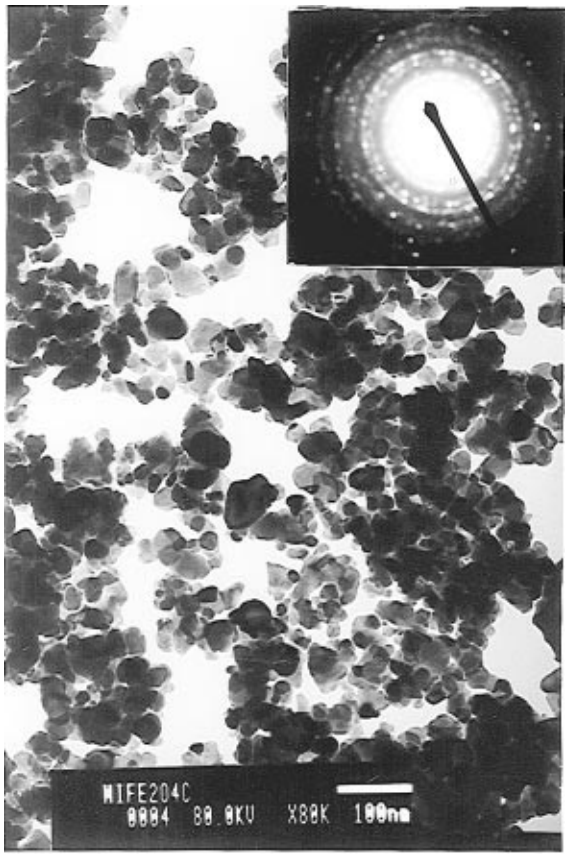

Figure 2. TEM image with microdiffraction (inset) for crystalline $NiFe_2O_4$.

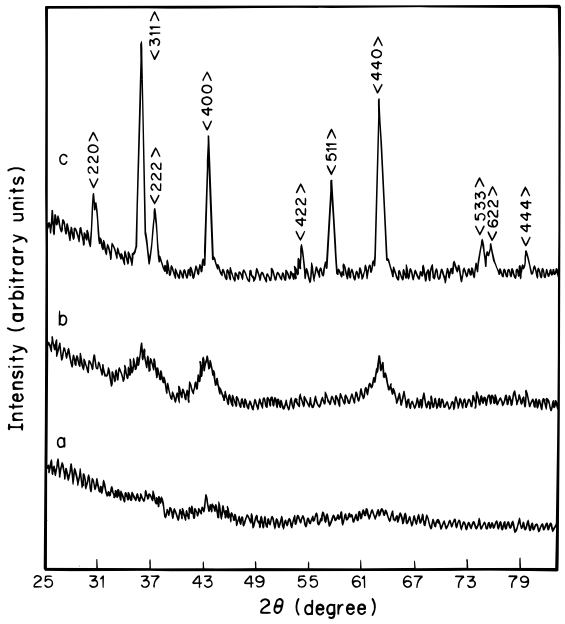

Figure 3. XRD patterns for $NiFe_2O_4$: (a) amorphous, (b) heated at 450 °C, and (c) heated at 700 °C.

lized. The XRD pattern for the amorphous as well as the heated samples of $NiFe_2O_4$ are shown in Figure 3. The X-ray diffractogram of the amorphous solid does not show any sharp diffraction patterns characteristic of crystalline phases. After heat treatment under pure argon (<10 ppm of O_2) at 450 °C for 5 h to induce crystallization, lines characteristic of $NiFe_2O_4$ start to appear (Figure 3b). The XRD pattern of the annealed sample (heated at 700 °C, Figure 3c) indicates that these nanoparticles have pure spinel structure, with all major peaks matching the standard pattern of bulk $NiFe_2O_4$ (JCPDS 10-325).

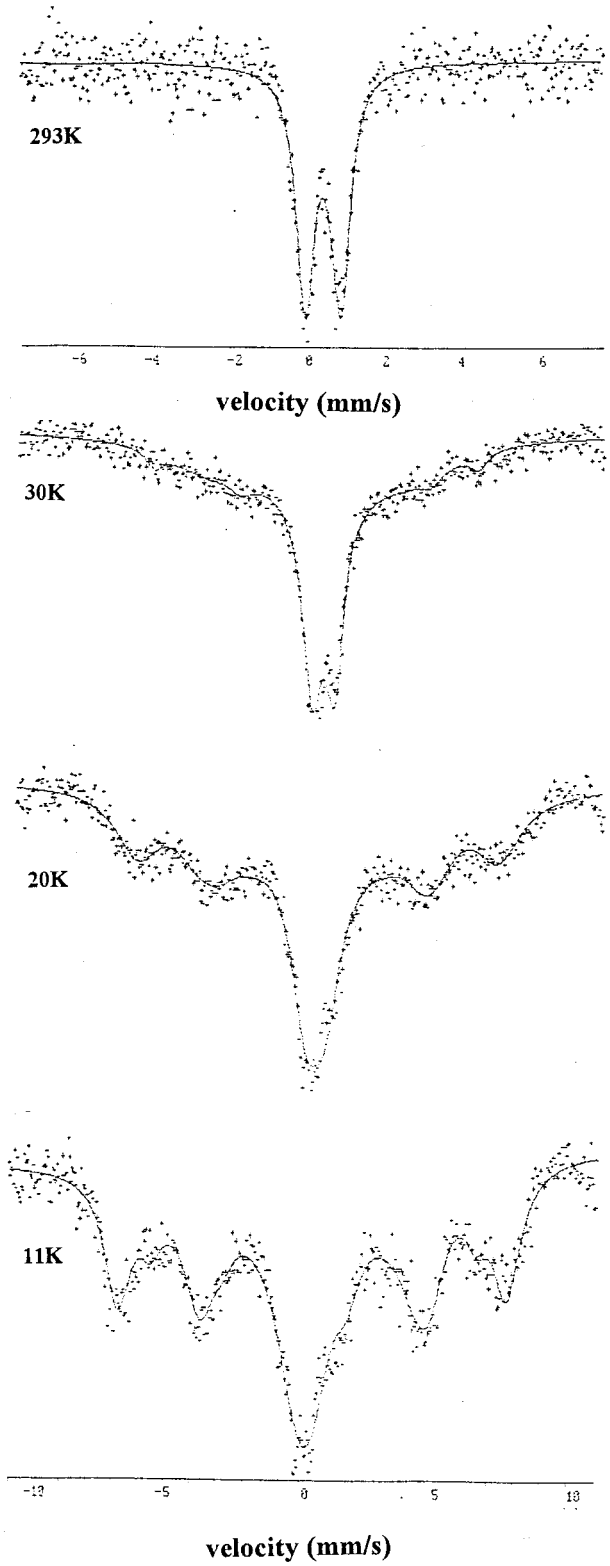

Figure 4. Low-temperature Mössbauer spectra of amorphous $NiFe_2O_4$ sample.

Mössbauer spectra of the amorphous $NiFe_2O_4$ at various temperatures are shown in Figure 4. The points represent the experimental results, and the computer-fitted data are shown as a solid line. The spectrum of the as-prepared sample shows a superparamagnetic quadrupole doublet at room temperature. On cooling, the spectrum shows broad features, and the magnetic sextet pattern emerges below 30 K. This suggests that the as-prepared ferrite nanoparticles are superparamagnetic with blocking temperature (the temperature above which the material is

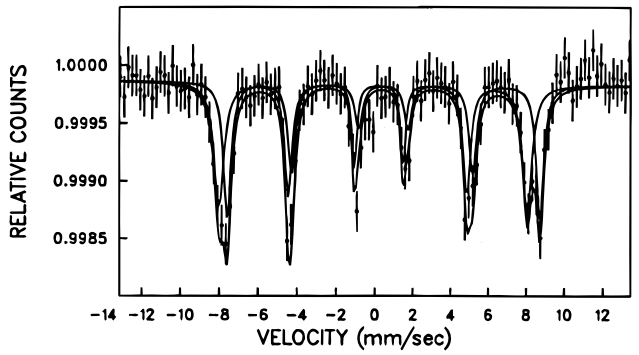

Figure 5. Room-temperature Mössbauer spectrum of the annealed sample of $NiFe_2O_4$.

superparamagnet) below 30 K. When the particle size of a ferro- or ferrimagnetic material becomes less than a critical value, d_{cr}, the material behaves like a paramagnet, with no saturation of magnetization and remanence in the hysterisis loop.[30,31] The critical value is determined by the energy balance, i.e., when the magnetic domain formation energy (proportional to the surface area) becomes larger than the energy of the magnetic self-field (proportional to the particle volume). Such a state of the magnetic material is called superparamagnetism.

The room temperature spectrum obtained after heating the ferrite at 700 °C and cooling to room temperature is shown in Figure 5. The spectra were fitted into six-line hyperfine patterns corresponding to ^{57}Fe in A (tetrahedral) and B (octahedral) sublattices. The sublattice hyperfine field and the other Mössbauer parameters are listed in Table 1. The hyperfine field values for the two sites, A (tetrahedral) and B (octahedral), are 500(1) and 508(1) kOe, respectively. The corresponding isomer shift values are 0.13 and 0.54 mm/s relative to metallic Fe. The lower value of the tetrahedral A site isomer shift value is typical of the difference between tetrahedral and octahedral coordination of Fe^{3+} in ferrites. Increased covalency at the tetrahedral site causes an increased s-electron density because of reduced shielding and thus reduces the isomer shift value.[32] The A and B hyperfine field values obtained are lower than those reported for bulk ferrite material ($H_A = 511 \pm 5$ kOe, $H_B = 553 \pm 5$ kOe).[32,33] The decrease of H_{eff} from the bulk value can be attributed to very small particle size effect. It is known that the magnetic properties, i.e., the saturation magnetization and the magnetic hyperfine field value, of nanoparticles are much smaller than those of the corresponding bulk materials.[29,30,34−36] Pannaparayil et al. have observed an hyperfine field value, $H_A = 505$ kOe, $H_B = 513$ kOe for the ultrafine nickel ferrite particles prepared by the hydrothermal process.[34]

The BET surface areas of the amorphous, as well as the crystallized (heated), samples of $NiFe_2O_4$ are given in Table 1. The surface areas of the amorphous and the crystallized (annealed) samples of $NiFe_2O_4$, 107 and 46 m^2/g, respectively, corroborate the Mössbauer spectroscopic studies. On annealing, the subdomain superparamagnetic nanoparticles become multidomain magnetic particles, thus yielding the magnetic split spectrum. The decrease in surface area of the heated sample is due to the increase in particle size by sintering.

Room temperature magnetization curves of the as-prepared and annealed samples of $NiFe_2O_4$ are shown in Figure 6. The curve of the amorphous sample does not reach saturation even at a magnetic field of 15 kG, and no hysterisis is found, indicating that the as-prepared (amorphous) $NiFe_2O_4$, particles are superparamagnetic. The observed value of saturation magnetization of the annealed sample (25 emu/g) is significantly lower than that for the reported multidomain bulk particles (55 emu/g). Cobalt ferrite, $CoFe_2O_4$, an inverse spinel, has a

TABLE 1: Mössbauer and EPR Parameters and Surface Areas of Amorphous and Crystallized (Annealed) Samples of $NiFe_2O_4$

	crystalline		
	A site	B site	amorphous
(a) Mössbauer			
line width	0.24(5)	0.47(5)	0.58(2)
isomer shift	0.13(1)	0.54(1)	0.35(1)
quadrupole shift,	0.11(1)	0.13(1)	0.91(1)
hyperfine field, H_{eff}	500(1)	508(1)	
ratio of intensity	55(5)	45(5)	
(b) EPR			
line width, ΔH_{pp} (G)	923		393
g factor, g_{eff}	2.37		2.10
suface area (m^2/g)	46		107

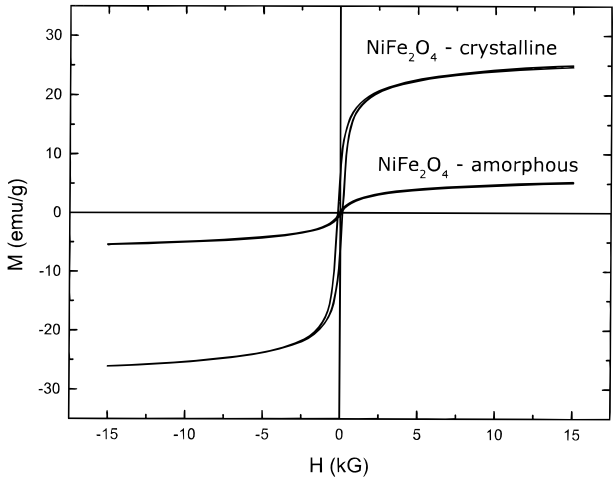

Figure 6. Room-temperature magnetization curves of $NiFe_2O_4$.

collinear ferrimagnetic spin structure in the bulk form. In the range 10−100 nm particle size, the decrease in the saturation magnetization has been explained in terms of its noncollinear spin arrangement at or near the surface of the particle.[37] Nickel ferrite, also an inverse spinel ferrimagnet, is known to have noncollinear magnetic structure when it is in the fine particle form.[6] Such a noncollinear structure attributed to a surface effect is more pronounced for the smaller particle size of our sample (<25 nm). The simplest description of a superparamagnetic material in a magnetic field employing Boltzmann statistics results in the Langevin function,[30] i.e., $M = M_s\{\coth(\mu H/kT) - (kT/\mu H)\}$, where M is the total magnetic moment of the particles per unit volume, μ is the magnetic moment of a single nanoparticle, and M_s is the saturation magnetization: $M_s = n\mu$, where n is the number of particles per unit volume. Fitting directly the Langevin function to our data, we estimated the mean diameter of the magnetic particles in amorphous sample, d, ~ 7 nm, which is in good agreement with the average particle size shown in the TEM micrograph (Figure 1).

Room temperature ESR spectra of the $NiFe_2O_4$ particles of both as-prepared (amorphous) and heated (crystallized) samples are shown in Figure 7. Figure 8 shows the room and low temperature spectra of the amorphous sample, heated at 150 °C under high vacuum (2×10^{-5} Torr) for 3 h, to remove the adsorbed impurities (see below). The spectra of the heated and unheated amorphous sample look similar. This indicates that the adsorbed impurity does not play any role in the EPR spectrum of the amorphous sample. The resonance line width ΔH_{pp} is defined as peak-to-peak distance, and the effective g factor is defined experimentally as $h\nu/\beta H$, where ν is the microwave frequency, H is the magnetic field at which the resonance maximum occurs, h is Planck's constant, and β is the Bohr magneton.

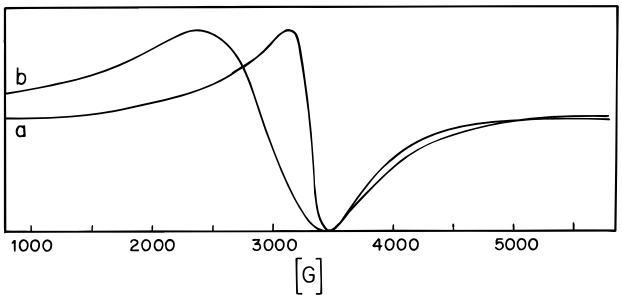

Figure 7. Room-temperature EPR spectra of $NiFe_2O_4$: (a) amorphous and (b) crystalline.

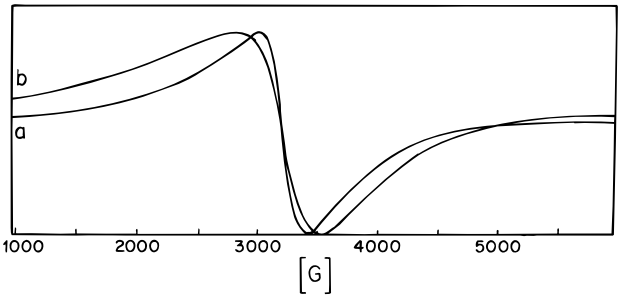

Figure 8. EPR spectra of the amorphous $NiFe_2O_4$: (a) at room temperature and (b) at 147 K.

The spectrum of the amorphous sample at room temperature (293 K) shows a relatively narrow signal with line width ΔH_{pp} = 393 G and the effective g value calculated to be 2.10. As the temperature is decreased to 147 K, the signal gets broadened, with no shift in the resonance magnetic field. The as-prepared, amorphous $NiFe_2O_4$ sample has shown superparamagnetic behavior in both magnetic and Mössbauer studies. The direction of magnetization in superparamagnetic particles fluctuates at a rate faster than the Larmor frequency, resulting in a narrow resonance line due to an averaging effect of this fluctuation on the magnetocrystalline anisotropy. Komatsu et al.[38] have observed a resonance signal, with line width of 130 G and effective g value of 2.12, for the $NiFe_2O_4$ as precipitated from silicate glass. For single-crystal $NiFe_2O_4$, a line width of 50 G is reported. The strong interparticle dipolar interactions in our as-prepared sample may dominate the average anisotropic field, thus leading to a relatively broad signal. As we see in the TEM micrographs, the nanostructured amorphous $NiFe_2O_4$ particles are highly agglomerated, causing strong dipolar interactions. The effective g value of 2.10 is in good agreement with that reported by Komatsu et al. The g value for the superexchange coupled pair between Fe^{3+} and Ni^{2+} ($Fe^{3+}-O-Ni^{2+}$) would be approximately 2.10 because the spectrum for Ni^{2+} ions normally give a g value in the range 2.2−2.3, and for Fe^{3+} it generally gives 2.0. The spectrum of the Fe^{3+} coupled pair ($Fe^{3+}-O-Fe^{3+}$) is known to give a line with $g_{eff} = 2.0$. So, the effective value obtained, $g_{eff} = 2.10$, seems to favor the $Fe^{3+}-O-Ni^{2+}$ rather than the $Fe^{3+}-O-Fe^{3+}$ in Fe_2O_3 or Ni^{2+} in NiO. A weak signal is also observed at about $g = 4.3$, in addition to the intense spectral line centered around $g = 2.10$. In oxide glasses,[39] containing ≥3 mol % of Fe_2O_3, a weak signal is observed with a g value of around 4.3, apart from the intense one centered around 2.0, and they are ascribed to an isolated Fe^{3+} in the orthorhombic field and to $Fe^{3+}-O-Fe^{3+}$ spin pair, respectively. This suggests that the as-prepared $NiFe_2O_4$ sample may have an impurity of Fe_2O_3 in an EPR detectable level of 3 mol %. The signal at $g = 2.0$ for Fe_2O_3 could be merged with the broad and intense peak for $NiFe_2O_4$ at $g = 2.10$. With decrease in the temperature (i.e., at 147 K), the line width resulting from interparticle magnetic dipolar interaction increases, as the averaging effect of thermal fluctuations of the direction of magnetization is reduced.

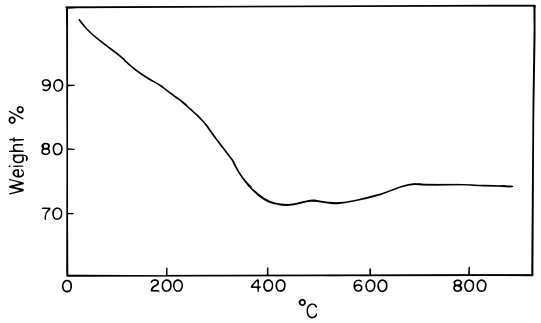

Figure 9. Magnetic force measurements on amorphous $NiFe_2O_4$.

The EPR spectrum of the annealed sample shows a resonance spectrum with a marked increase in line width and g value, i.e., $\Delta H_{pp} = 923$ and $g_{eff} = 2.37$. Siu et al.[5] have observed a g value of 2.43 for the polycrystalline $NiFe_2O_4$. For a single crystal, the reported value is 2.21.[40] The increased magnetic field produced by the magnetocrystalline anisotropy, as well as the interparticle dipolar interaction, is the reason for the high g value. For ferrimagnetic particles, the intrinsic moments are large (2.2 μ_B for $NiFe_2O_4$), so the magnetic dipolar interactions among these particles are strong, thus increasing the value of ΔH_{pp} and g_{eff}.

Figure 9 shows the result of a magnetic force measurement, obtained with a thermogravimetric balance, on amorphous $NiFe_2O_4$ powder. The percentage change in weight is plotted as a function of increasing temperature. The early decrease in weight is due to the removal of adsorbed impurities. The IR spectrum of the as-prepared amorphous material shows peaks characteristic of adsorbed carbonyls (peak around 2050 cm^{-1}) and the hydrocarbon solvents (decane and pentane, peaks around 2950, 1475, and 1350 cm^{-1}) impurities in small detectable level. This is reasonable because these nanostructured amorphous materials are known to be highly porous, as they are seen on TEM micrographs as agglomerates of small particles with average diameters of less than 10 nm. The amorphous sample has a Curie temperature T_c of 440 °C, followed by a higher T_c at 560 °C, associated with the crystalline form. The broad nature of the Curie transition peaks can be attributed to a probable distribution of the particle size. The decrease of T_c of the crystalline form from the bulk value (585 °C) is due to the ultrafine nature (small particle size effect) of the sample. As the particle size decreases, its surface to volume ratio increases, giving raise to more number of atoms sitting on the surface lacking the complete coordination. This leads to a reduction in the magnetic ordering, which is manifested in the decreased value of ferrimagnetic ordering temperature (Curie temperature, T_C).[41]

The result of DSC measurement of the amorphous particle is shown in Figure 10. Surprisingly, the exothermic peak characteristic of crystallization was not observed. Instead, three endotherms—a wide one centered around 100 °C, a small and narrow one with peak minimum at 212 °C, and the third, strong and wide with peak minimum at 342 °C—were observed. We ran the DSC of the sample $NiFe_2O_4$ in two scans. The first involved heating to 500 °C at a rate of 10 °C/min. After cooling the sample to room temperature, in the second scan, the sample was again heated to 500 °C at a rate of 10 °C/min. We observed that all the peaks vanished in the second DSC scan. We are thus satisfied that the first two endothermic peaks are due to the desorption of the impurities. We assume that the wide endothermic peak at 342 °C has to do with magnetic transition,

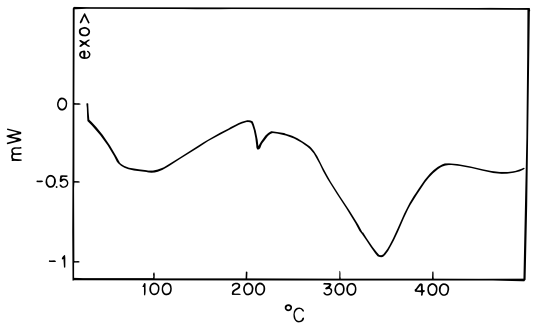

Figure 10. Differential scanning calorimetric curve of the amorphous $NiFe_2O_4$.

though we do not find a corresponding sharp inflection point (of increase in weight) in the TG curve with magnet (Figure 9). The endothermicity of the magnetic transition (Curie) dominates over the usual exothermicity of the amorphous-to-crystalline transition, resulting in a net endothermic peak near 342 °C. Similar behavior was observed earlier for the amorphous Fe−Ni alloy,[29] where the endothermic peak temperature was nearly matching with the Curie temperature of the magnetic transition. A systematic and detailed study is required, since the thermal behavior of the alloy particles is very sensitive to the history of the sample preparation, as well as to the thermal procedures, like annealing temperature and heating rate.

Conclusions

Sonochemical decomposition of the solutions of volatile organic precursors, $Fe(CO)_5$ and $Ni(CO)_4$ in decalin at 273 K, under an oxygen pressure of 100−150 kPa (1−1.5 atm), yields amorphous, nanosized $NiFe_2O_4$ particles. Magnetic data, Mössbauer, and EPR spectral studies indicate the superparamagnetic nature of the as-prepared amorphous and also the ultrafine nature of the crystallized sample.

Acknowledgment. This research was supported by Grant 94-00230 from the U.S.−Israel Binational Science Foundation (BSF), Jerusalem. We thank the Israeli Ministry of Science and Arts for the Binational Indo-Israel Grant. A. Gedanken is grateful to the Bar-Ilan Research Authorities for supporting this project. Prof. Lendvai and Dr. Koltypin thank the Israeli and Hungarian Ministries of Science for awarding them a scientific exchange grant. R. Prozorov acknowledges a support from the Clore Foundations. Also, we thank Prof. M. Deutsch for use of X-ray diffraction facilities and Prof. Y. Yeshurun for extending facilities of National Center for Magnetic Measurements at the Department of Physics, Bar-Ilan University. We are grateful to Prof. Margel for the TG-DSC measurements.

References and Notes

(1) Kuliokowski, J.; Lenniewski**,** A. *J. Magn. Magn. Mater*. **1980,** *19*, 117.
(2) Igarashi, H.; Okozaki, K. *J. Am. Ceram. Soc*. **1977**, *60*, 51.
(3) Ozin, G. A. *Adv. Mater*. **1992**, *4*, 612.
(4) Gleiter, H. *Adv. Mater*. **1992**, *4*, 474.
(5) Sui, Y.; Xu, D. P.; Zheng, F. L.; Su, W. H. *J. Appl. Phys*. **1996**, *80* (2), 719.
(6) Morrish, A. H.; Haneda, K. *J. Appl. Phys*. **1981**, *52* (3), 2496.
(7) Bee, A.; Massart, R.; Neveu, S. *J. Magn. Magn. Mater*. **1995**, *149*, 6.
(8) Yu, H-F.; Gadalla, A. M. *J. Mater. Res.* **1996**, *11* (3), 663.
(9) Pannaparayil, T.; Marande, R.; Komarneni, S. *J. Appl. Phys*. **1991**, *69* (8), 5349.
(10) Kodama, R. H.; Berkowitz, A. E.; McNiff, Jr., E. J.; Foner, S. *Phys. Rev. Lett*. **1996**, *77* (2), 394.
(11) Noumeni, N.; Veillet, P.; Pileni, M. P. *J. Magn. Magn. Mater*. **1995**, *149*, 67.
(12) Kommareddi, N. S.; Tata, M.; John, V. T.; McPherson, G. L.; Herman, M. F.; Lee, Y.-S.; O'Connor, C. J.; Akkara, J. A.; D. L. Kaplan, *Chem. Mater*. **1996**, *8*, 801.
(13) Tanaka, K.; Hirao, K.; Soga, N. *J. Appl. Phys*. **1991**, *69* (11), 7752.
(14) Sugimoto, M.; Hiratsuka, N. *J. Magn. Magn. Mater*. **1983**, *31*−*34*, 1533.
(15) Sugimoto, M. *J. Magn. Magn. Mater*. **1994**, *133*, 460.
(16) Suslick, K. S. *Science* **1990**, *247*, 1439.
(17) Flint, E. B.; Suslick, K. S. *Science*, **1991**, *253*,1397.
(18) Atchley, A. A.; Crum, L. A. In *Ultrasound, its Chemical, Physical and Biological Effect*; Suslick, K. S., Ed.; VCH Press: NewYork, 1988.
(19) Greer, A. L. *Science* **1995**, *267*, 1947.
(20) Suslick, K. S.; Hammerton, D. A.; Cline, Jr., R. E. *J. Am. Chem. Soc*. **1986**, *108*, 5641.
(21) Suslick, K. S.; Choe, S.-B.; Cichowlas, A. A.; Grinstaff, A. A. *Nature* **1991**, *353*, 414.
(22) Grinstaff, M. W.; Salmon, M. B.; Suslick, K. S. *Phys. Rev. B* **1993**, *48*, 269.
(23) Bellissent, R.; Galli, G.; Hyeon, T.; Magazu, S.; Majolino, D.; Migliardo, P.; Suslick, K. S. *Phys. Scr*. **1995**, *T57*, 79.
(24) Suslick, K. S.; Hyeon, T.; Fang, M. *Chem. Mater*. **1996**, *8*, 2172.
(25) Suslick, K. S.; Hyeon, T.; Fang, M.; Cichowlas, A. A. *Mater. Sci. Eng.* **1996**, *A204*, 186.
(26) Koltypin, Yu.; Katabi, G.; Cao, X.; Prozorov, R.; Gedanken, A. *J. Non-Cryst. Solids* **1996**, *201*, 159.
(27) Cao, X.; Koltypin, Yu.; Kataby, G.; Prozorov, R.; Gedanken, A. *J. Mater. Res.* **1995**, *10*, 2952.
(28) Cao, X.; Prozorov, R.; Koltypin, Yu.; Kataby, G.; Felner, I.; Gedanken, A. *J. Mater. Res.* **1997**, *12*, 402.
(29) Shafi, K. V. P. M.; Gedanken, A.; Goldfarb, R. B.; Felner, I. *J. Appl. Phys.* **1997**, *81* (10), 6901.
(30) Moumen, N.; Pileni, M. P. *J. Phys. Chem*. **1996**, *100*, 1867.
(31) (a) Cullity, B. D. *Introduction to Magnetic Materials*; Addison Wesley: Reading, MA, 1972. (b) Craik, D. *Magnetism, Principles and Applications*; John Wiley & Sons: Chichester, England, 1995.
(32) Greenwood, N. N.; Webb, T. G. *Mössbauer Spectroscopy*; Chapman and Hall: London, 1971.
(33) Leung, L. K.; Evans, B. J.; Morrish, A. H. *Phys. Rev*. **1973**, *B8*, 29.
(34) Pannaparayil, T.; Marande, R.; Komarneni, S.; Sankar, S. G. *J. Appl. Phys*., **1988**, *64* (10), 5641.
(35) Morup, S.; Dumesic, J. A.; Topsøe, H. In *Mössbauer Spectroscopy, Applications*; Cohen, R. L., Ed.; Academic Press: New York, 1990; p 1.
(36) Jiang, X.; Stevenson, S. A.; Dumesic, J. A.; Kelly, T. F.; Casper, R. J. *J. Phys. Chem.* **1984**, *88*, 6191.
(37) Haneda, K.; Morrish, A. H. *J. Appl. Phys.* **1988**, *63* (8), 4258.
(38) Komatsu, T.; Soga, N.; Kanugi, M. *J. Appl. Phys*. **1979**, *50(10)*, 6469.
(39) Tanaka, K.; Kamiya, K.; Yoko,T.; Tanabe, S.; Hirao, K.; Soga, N. *J. Non-Crys. Solids* **1989**, *109*, 289.
(40) Miyamoto, S.; Tanaka, N.; Iida, S. *J. Phys. Soc. Jpn*. **1965**, *20*, 753.
(41) Murad, E. *Phys. Chem. Miner.* **1996**, *23*, 248.